Synthesis of Size-Tunable Anatase TiO₂ Nanospindles and Their Assembly into Anatase@Titanium Oxynitride/Titanium Nitride—Graphene Nanocomposites for Rechargeable Lithium Ion Batteries with High Cycling Performance

Yongcai Qiu,[†] Keyou Yan,[†] Shihe Yang,[†,*] Limin Jin,[‡] Hong Deng,[‡] and Weishan Li[‡]

[†]Nano Science and Technology Program, Department of Chemistry, William Mong Institute of Nano Science and Technology, The Hong Kong University of Science and Technology, Clear Water Bay, Kowloon, Hong Kong, China, and [‡]School of Chemistry & Environment and Key Laboratory of Electrochemical Technology on Energy Storage and Power Generation of Guangdong Higher Education Institutes, South China Normal University, Guangzhou 510006, China

Lithium ion batteries (LIBs), as energy storage devices dominating power sources for portable electronics and electrical/hybrid vehicles, have attracted considerable attention in the scientific and industrial communities.[1] The ever-growing market demand for their high electromotive force, high energy density, and high cyclability has stimulated numerous research efforts aimed at the development of new high performance electrode materials for LIBs.[2−4] TiO₂ has received special interest for LIBs for several reasons. First, TiO₂ is itself not only a fast and low voltage insertion host for Li, but also an abundant, low cost, and environmentally benign electrode material.[5−10] Second, during Li insertion/extraction, TiO₂ can remain structurally stable and free of electrochemical Li deposition, which is vital for the safe operation of LIBs. However, the cycling performance of TiO₂ electrodes at high discharge/charge rates is still poor owing to the poor electron transport in TiO₂ and the aggregation tendency of TiO₂ nanoparticles.[11] Efforts have already been spent to address this problem by using hybrid nanostructured electrodes, for example, anatase TiO₂/RuO₂ nanocomposite,[12] which used conductive additives to interlink the TiO₂ nanostructures so as to improve the Li ion insertion performance. Aside from the enhancement of electron transport, a carbon coating onto nanoparticles has an added advantage of

suppressing their aggregation during cycling, hence increasing the Li-ion insertion/extraction capacity of the hybrid electrodes at high discharge/charge rates.[13] However, the extent of dispersion and conductivity increase of the active materials is still rather limited.
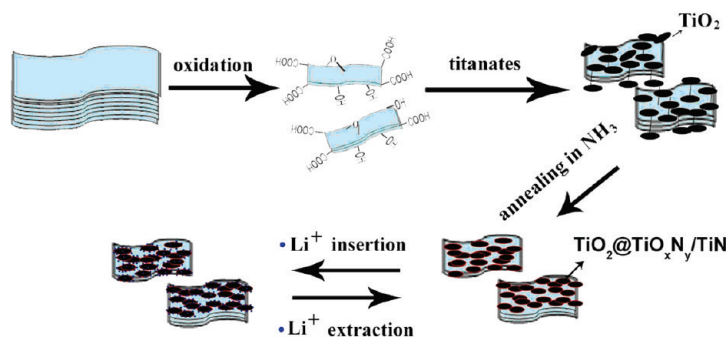
One-dimensional (1D) metal oxide nanostructured materials such as nanowires, nanotubes, and nanorods are particularly interesting in LIBs owing to, save for the large surface to volume ratio, their

ABSTRACT This paper embarks upon three levels of undertaking ranging from nanomaterials synthesis to assembly and functionalization. First, we have prepared size-tunable anatase TiO₂ nanospindles *via* a hydrothermal process by using tubular titanates as self-sacrificing precursors. Second, we have densely dispersed the TiO₂ nanospindles onto functional graphene oxides (GO) *via* a spontaneous self-assembly process. After annealing of the TiO₂/GO hybrid nanocomposite in an NH₃ gas flow, the TiO₂ surface was effectively nitridated and the GO was reduced to graphene sheets (GS) in order to further fortify the electronic functionality of the nanocomposite. Third, the anatase@oxynitride/titanium nitride-GS (TiO₂@TiOₓNᵧ/TiN—GS) hybrid nanocomposite was studied as an anode material for lithium-ion batteries (LIBs), showing excellent rate capability and cycling performance compared to the pure TiO₂ nanospindles. Our systematic studies have revealed that the TiO₂@TiOₓNᵧ/TiN—GS nanocomposites with graphene nanosheets covered with the TiO₂@TiOₓNᵧ/TiN nanospindles on both sides provide a promising solution to the problems of poor electron transport and severe aggregation of TiO₂ nanoparticles by enhancing both electron transport through the conductive matrix and Li-ion accessibility to the active material from the liquid electrolyte. More generally, the size-tunable TiO₂ nanospindles with their unique (101) outer surface planes provide an archetype for the in depth investigation of their surface-specific and size-dependent physicochemical properties.

KEYWORDS: anatase nanospindles · TiO₂@TiOₓNᵧ/TiN—graphene nanocomposite · anode · lithium ion batteries

Scheme 1. Scheme for the synthesis and the subsequent lithiation/delithiation processes of the TiO$_2$@Ti$_x$O$_y$/TiN$-$GS nanocomposites.

vectorial ion and electron transport and apt accommodation of lithiation induced stresses.[14$-$25] To date, considerable efforts have been devoted to the synthesis of TiO$_2$ nanomaterials with various morphologies through different methods such as sol, sol$-$gel, micelle, and inverse micelle, hydrothermal/solvothermal methods.[26] Among the studies, few have reported the synthesis of anatase TiO$_2$ nanospindles.[27,28] Yang *et al.* synthesized anatase TiO$_2$ nanospindles through hydrothermal treatment of titanium isopropoxide and triethyl amine.[29] Wang *et al.* achieved hydrothermal preparation of anatase TiO$_2$ nanoshuttles under alkaline conditions by employing titanate nanowires as the source precursors.[30] However, only large size nanospindles could be obtained in these works, with diameters of 20$-$150 nm and lengths of 200$-$300 nm, which may put a bar on their applications in LIBs.

In the work reported here, we have succeeded in the synthesis of spindle-like TiO$_2$ with tunable diameters down to 5 nm and lengths of about 15 nm by hydrothermally transposing a titanate nanotube precursor in the presence of alkyl amines and a variant viscosity solvent. Such size-tunable TiO$_2$ nanospindles are featured by large exposed (101) surfaces, which could be a fertile ground for systematic exploration of size-dependent photocatalysis, gas sensing, dye-sensitized charge separation/recombination and lithium ion insertion/extraction.[17$-$21] We have further densely immobilized the ultrafine, surface-nitrided TiO$_2$ nanospindles onto graphene nanosheets with the merit that high dispersion of the active material in a highly conductive matrix would curb particle aggregation and dramatically boost the cycling performance of LIBs at high discharge/charge rates. On one hand, the high electronic conductivity of graphene sheets can assist the storage of Li$^+$ in TiO$_2$ by providing rapid access to electrons. On the other hand, the large surface area of graphene sheets allows the easy access of Li$^+$ ions from the liquid electrolyte to TiO$_2$ on both sides of the graphene sheets. Recently, graphene sheets, with superior electrical conductivities, high specific surface areas of over 2600 m^2/g, and excellent structural stability,[31$-$34] have emerged as a new conductive matrix for dispersing electrochemically active metal oxides for develop-

ing hybrid nanostructured LIB electrodes.[35,36] However, the active material dispersion was still inadequate, and furthermore, it is yet to be extended to other materials such as TiO$_2$.[37] The present work is intended to address this gap. We have tested the nitridation-driven conductive anatase@titanium oxynitride/titanium nitride (TiO$_2$@TiO$_x$N$_y$/TiN) onto graphene sheets (GS) as potential LIB anode materials, and demonstrated significantly enhanced cycling performance, especially at high discharge/charge rates. Scheme 1 illustrates an overview of the present work.

RESULTS AND DISCUSSION

Formation of TiO$_2$ Nanospindles. The TiO$_2$ nanospindles were prepared by hydrothermal treatment of a source precursor—titanate nanotubes—in the presence of alkyl amines. The precursor was synthesized by a simple hydrothermal reaction of NaOH and TiO$_2$, followed by acid washing, as described in the Experimental Details section.[38] SEM and TEM images of the precursor are shown in Figure 1 panels a and b, respectively, confirming a distinct tubular morphology with an average diameter of ~10 nm and lengths ranging from hundreds of nanometers to a few micrometers. XRD patterns in Figure 2a,b show clearly that the precursor (titanates) has been transformed to anatase TiO$_2$ (JCPDS card no. 21-1272) after hydrothermal treatment under an alkaline condition. The sharp and strong XRD peaks for the as-prepared anatase TiO$_2$ attest the good crystallinity and high crystalline purity of the product. The as-prepared anatase TiO$_2$ was subjected to further structural characterizations. From the low magnification SEM image in Figure 1c, the as-prepared anatase TiO$_2$ displays exclusively a spindle-like nanostructure with a uniform size. More quantitatively, the diameters of 30$-$50 nm and the lengths of 200$-$300 nm for the nanospindles can be estimated from the high magnification SEM image in Figure 1d.

Shown in Figure 3a is the TEM image of a randomly chosen TiO$_2$ nanospindle with a high aspect ratio of ~7, and its corresponding HRTEM image taken near one of the tips is juxtaposed in Figure 3b. A lattice spacing of 3.5 Å is recognized and can be ascribed to the (101) planes of anatase TiO$_2$. The SAED pattern of the
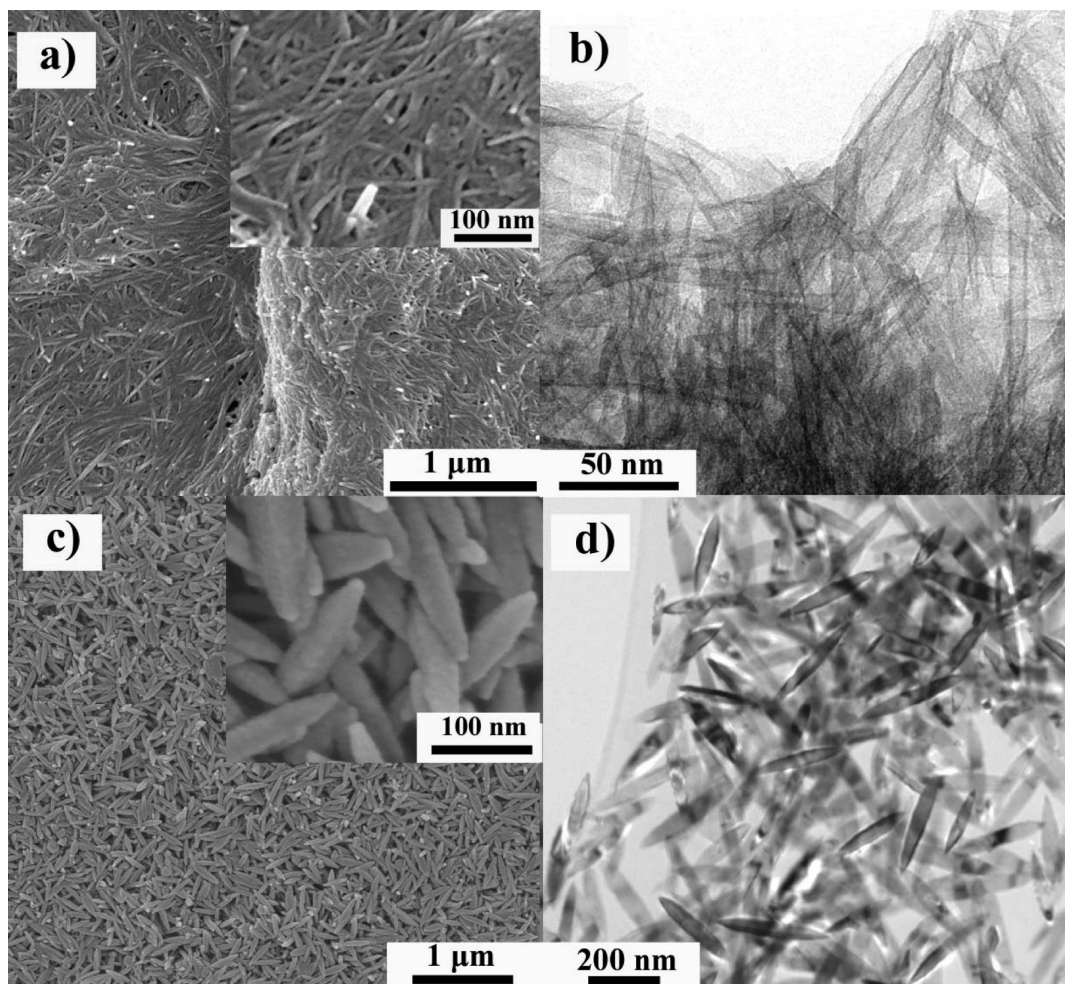
Figure 1. (a) Low and high magnification (inset) SEM images and (b) TEM image of the as-prepared titanate precursor. (c) Low and high magnification (inset) SEM images and (d) TEM image of the as-prepared TiO$_2$ nanaspindles.

nanospindle shows a set of well-defined spots, indicative of single-crystallinity. Also, by indexing the regular spots of this pattern, one finds a preferred growth direction of the nanospindle along the [001] axis. The tip is thus confined by one set of (101) outer surfaces, which are known to easily adsorb dimethylamines.[39,40]
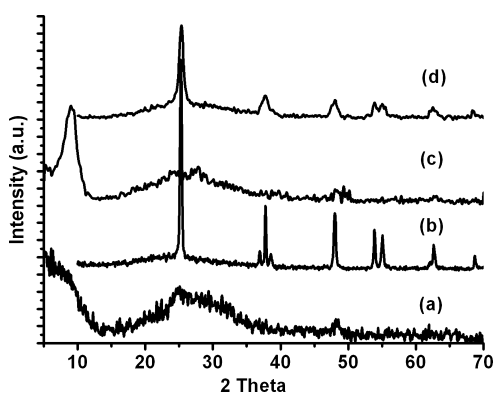

Figure 2. XRD patterns of as-prepared titanate precursors (a), TiO$_2$ nanospindles (b), hydrogen titanate hydrate (c), and the product after annealing of the hydrogen titanate hydrate (d).

Having established that the anatase TiO$_2$ nanospindles were indeed transformed from the tubular titanate precursors, the key question now is how this transformation occurred. To tackle this question, we performed experiments aiming to track the timing course of the transformation process. Figure 4 shows TEM images of a precursor sample after different periods of hydrothermal treatment but under otherwise identical reaction conditions in a mixture of ethanol and ethylene glycol (v/v = 1:1) in the presence of alkyl amines. Surprisingly, with increasing reaction time, more and more nascent nanospindles were formed and appeared to perpendicularly line up (side by side) along the precursor nanotubes (see Figures 4a−d). Eventually, the tubular structures vanished and were supplanted by abundant collections of nanospindles, as can be seen from Figure 4d.

Next, we found that the reaction solvent plays an important role in controlling the size of the TiO$_2$ nanospindles. In our experiments, we found that viscosity of the reaction solvent could be used to tune the sizes of the nanospindles. In Table 1, three TiO$_2$ nanospindle products are listed as SP-200, SP-100, and SP-20 with de-
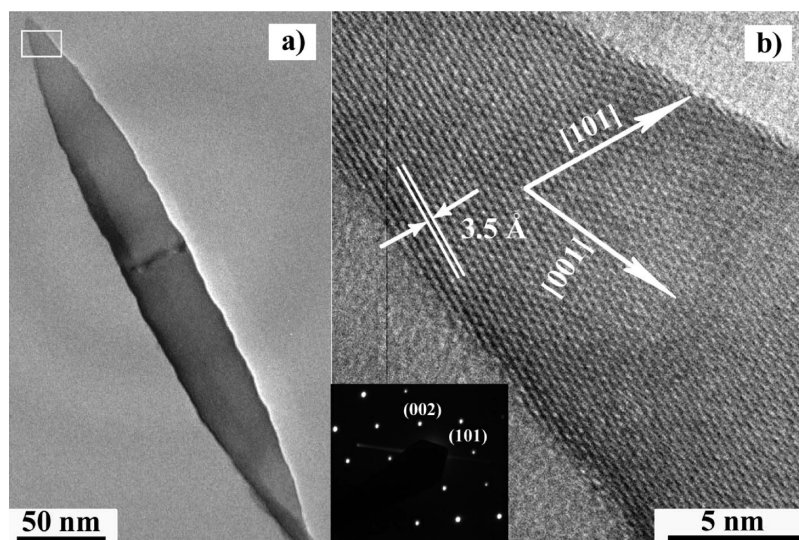
Figure 3. A typical TEM image (a) and HRTEM image (b) of the as-prepared TiO₂ nanospindles. Inset of panel b: SAED pattern.

creasing size in that order. In Figure 5, SEM and TEM images show the nanospindle size changes of the as-prepared products with addition of different amounts of ethylene glycol into the reaction system. Specifically, when the reaction media consisted of 50 mL of water and 10 mL of ethylene glycol, we obtained TiO₂ nanospindles with a mean diameter of 30 nm and a length of ∼100 nm (see Figure 5a,b). When the volume ratio of water/ethylene glycol was 1:2, the average diameter of the as-prepared nanospindles reduced to ∼10 nm and the mean length to ∼20 nm (see Figure 5c,d).

Some additional control experiments were also carried out. First, when no alkyl amines were used in the reaction, the tubular structure was maintained. Second,
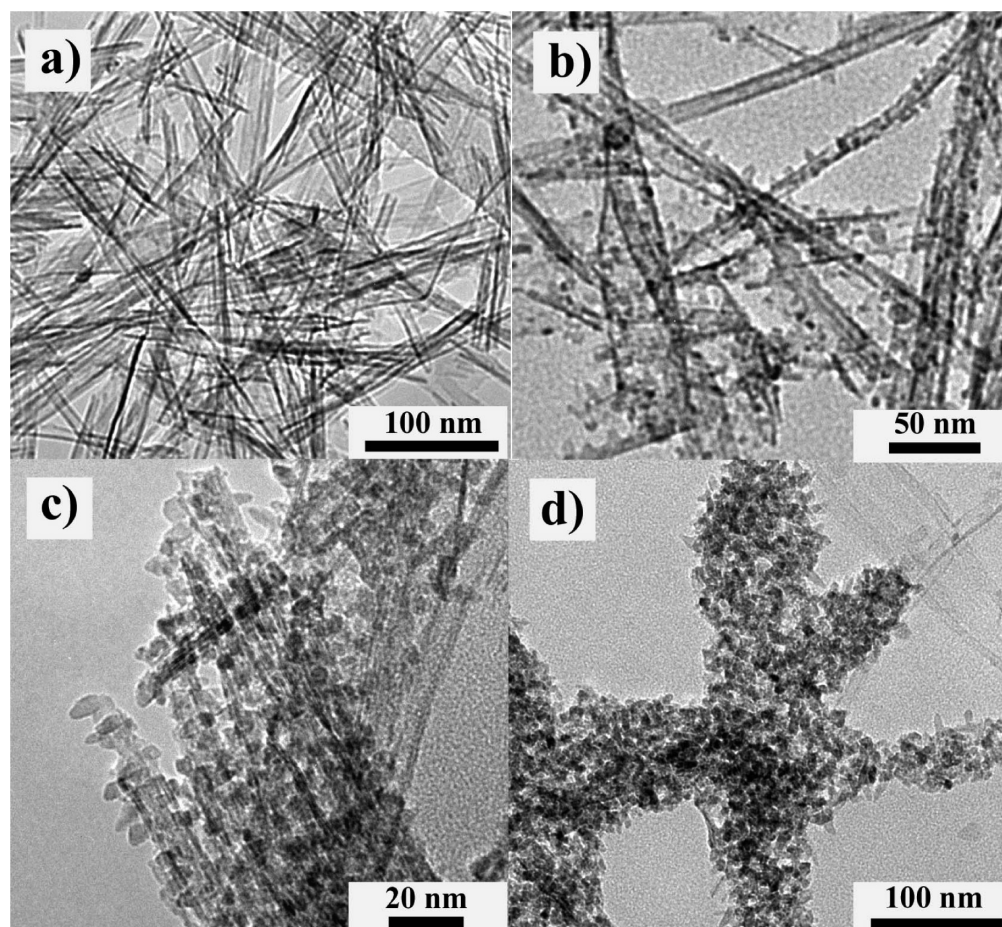

Figure 4. TEM images of the products obtained after different periods of reaction times: (a) 0, (b) 0.5, (c) 1.5, and (d) 3 h.

TABLE 1. Summary of the Synthesis Conditions and Sizes of the TiO$_2$ Nanospindles Obtained Using Different Solvents^a

samples	water (mL)	ethanol (mL)	EG (mL)	diameters (nm)	lengths (nm)
SP-200	30	30		30—50	200—300
SP-100	50		10	25—35	80—130
SP-20	20		40	6—15	15—25

^{a}The hydrothermal reactions were at 180 °C and lasted for 12 h. EG: ethylene glycol.

when the reaction was conducted by replacing water with DMF but under otherwise identical conditions, a sponge-like loose structure was observed with SEM (see Supporting Information, Figure S1a). The XRD pattern of the product shown in Figure 1c exhibits a new broad peak at around 9° when compared with that of the as-prepared titanate in Figure 1a, which can be attributed to hydrogen titanate hydrate (JCPDS card no. 47-0124). After annealing at 500 °C, the morphology was mostly changed and some sheets were cracked into smaller debris (see Supporting Information, Figure S1d). The resulting composition of the product was determined to

be anatase TiO$_2$ according to the XRD pattern in Figure 2d.

Our experiments, in conjunction with results reported previously by other researchers,[30,41] show that water and alkyl amines both play important roles in the formation of the spindle-like structure of TiO$_2$ and that the addition of ethylene glycol can leverage the size of the nanospindles. Accordingly, the formation mechanism of the TiO$_2$ nanospindles can be proposed, which involves a dissolution—nucleation process under hydrothermal conditions. This mechanism is in conformity to the observed large changes of morphologies from the nanotubes to the nanospindles.[41] As is well-known, each layer of the layered titanate is composed of corrugated ribbons of edge-shared TiO$_6$ octahedra, which are about three TiO$_6$ octahedra wide and laterally linked together through corner sharing, and separated by H$^+$ ions from the neighboring layers (see the crystal structure of H$_x$Ti$_3$O$_7$ in Scheme 2).[42−44] As such, the layered titanate could be easily delaminated, exfoliated, and split into discrete Ti monomer or oligomer units under the alkaline and hydrothermal condition. The Ti monomer or oligomer units would then be assembled into

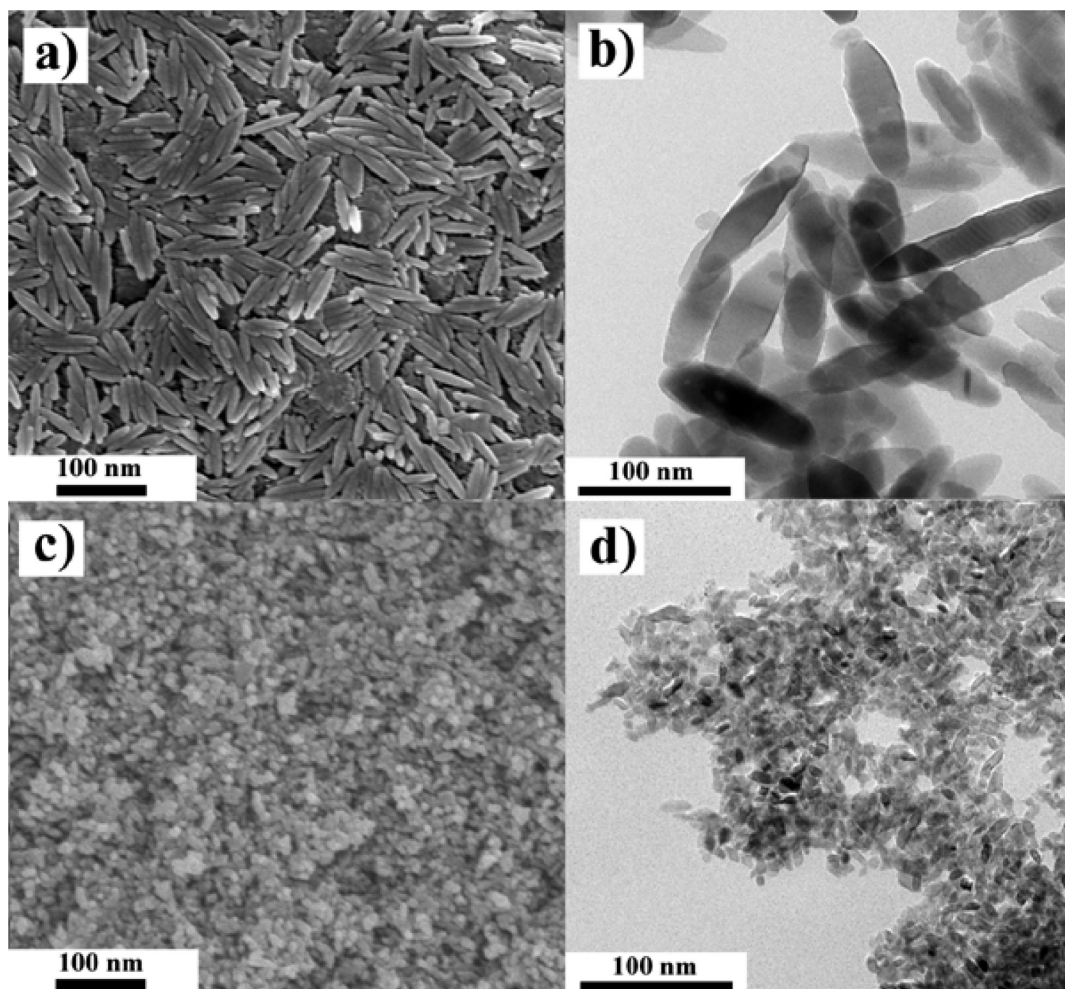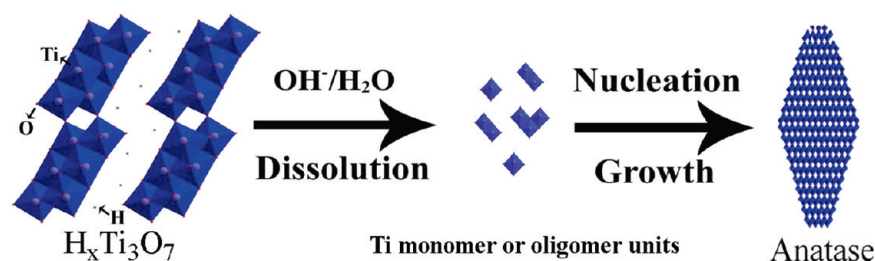

Figure 5. (a) A SEM image and (b) a TEM image of as-prepared spindles reacted in 50 mL of water and 10 mL of ethylene glycol. (c) A SEM image and (d) A TEM image of as-prepared spindles reacted in 20 mL of water and 40 mL of ethylene glycol.

Scheme 2. Schematic representation of a possible formation mechanism of the anatase nanospindles.

the anatase nanospindles. Such a proposition on the phase and shape transformation is consistent with our TEM observations (Figure 4a–d and XRD patterns in Figure 2). In the initial stage of reaction, the layer structured titanate nanotubes were gradually decomposed and produced Ti monomer or oligomer building units by hydrolysis, which could immediately nucleate and grow into anatase structure superseding the sacrificed titanate nanotube precursor under the alkaline condition (see Scheme 2). The dissolution process would happen from the outer to the inner titanate layer gradually, and this explains why the nucleation took place all over the titanate tubular surface simultaneously.[42] Moreover, the fact that the emerging nanospindles were perpendicularly attached onto the sacrificial nanotubes (see Figure 4b,c) can be explained by the scenario that the undissolved quasi-anatase nucleus on the tubular surface of the titanate could serve as seeds for the growth of spindle-shaped nanocrystals with their surfaces being capped by dimethylamine. As the reaction went on, all of the tubular titanates were gradually dissolved and finally transformed to the much smaller sized anatase nanospindles (Figure 4d). In addition, owing to its high viscosity, ethylene glycol as part of the solvent could reduce the rate of the spindle crystal growth in a reagent transport limited regime. As a support, only very small TiO_2 nanoparticles were obtained when pure ethylene glycol was used as the reaction solvent (see Supporting Information, Figure S2).

Assembly of TiO_2/Graphene Oxides Nanocomposites. To uniformly disperse the TiO_2 nanospindles onto graphene sheets, we first adopted a hydrothermal process to treat the titanate precursor and graphene oxides in the presence of alkyl amines. Of note, the graphene oxides synthesized by the modified Hummers method (see Experimental Details section) consist of basal plane carbon atoms decorated with epoxy and hydroxyl groups and edge carbon atoms attached by carbonyl and carboxyl groups, as vindicated by XPS and FT-IR spectra (see Supporting Information, Figure S3 and S4). The C 1s XPS spectrum (Figure 3b) shows two peaks at binding energies of *ca.* 283–290 eV, which are indicative of the existence of oxygen functionalities associated with the epoxy and hydroxyl groups as well as the carbonyl and carboxyl groups on the graphene sheets (see Supporting Information, Figure S3).[37,45] The FT-IR spectra further attest the existence of these functional groups in the

graphene oxides. The broad band at 3600−3100 cm^{-1} and the peak at around 1630 cm^{-1} correspond, respectively, to the stretching and bending modes of the structural OH groups and of the OH groups of adsorbed water. The weak band located at 1730−1710 cm^{-1} can be assigned to the stretching vibration of carboxyl groups on the edges of the sheets.[46] The bands at around 1345 and 1060 cm^{-1} are associated with to the vibrations of C−OH and C−O groups, respectively (see Supporting Information, Figure S4). Such functional groups are important sites for interlinking the graphene sheets to TiO_2 nanospindles. Indeed, after reaction with graphene oxides in the presence of alkyl amines, the titanate nanotubes were transformed into TiO_2 nanospindles which were then anchored *via* these functional groups onto the surface of graphene oxides, as shown in a typical TEM image in Figure 6a. The attached TiO_2 nanospindles are well-defined and have on average a uniform diameter of ~10 nm and length of ~20 nm. After annealing the as-formed nanocomposite in NH_3 atmosphere, the morphology was largely conserved, as shown in Figure 6b. The purpose of such annealing in NH_3 is 2-fold. First, the graphene oxide sheets can be transformed into N-doped graphene sheets, which have been confirmed by a sharp C 1s XPS peak at ~285.4 eV (see Supporting Information, Figure S3), typical of a good sp^2-type π-conjugation in the graphene sheets, and an N 1s XPS peak at ~398.7 eV (see inset in Figure 7b), suggestive of the C−N bond formation in the graphene sheets. In fact, Dai *et al.* already demonstrated that annealing in NH_3 is more effective in enhancing the conductivity of graphene oxides (GO) than the hydrazine solvothermal reduction treament.[47] Second, an ultrathin conductive TiN/TiO_xN_y layer is expected to form on the surface of the TiO_2 nanospindles,[48] as will be discussed below.

The Raman spectrum of the $TiO_2@TiO_xN_y/TiN$−GS nanocomposite is shown in Supporting Information Figure S5. The peaks at 150, 392, 515, and 631 cm^{-1} can be assigned as the E_g, B_{1g}, A_{1g}, or B_{1g}, and E_g modes of the anatase phase, respectively.[49] A weak peak at around 450 cm^{-1} and a shoulder peak at around 610 cm^{-1} (marked by an arrow) appeared after the thermal treatment at 650 °C, corresponding to the E_g and A_{1g} modes of the rutile phase. The D and G bands at around 1350 and 1580 cm^{-1}, respectively, correspond to the structure of carbon, indicating that the structure of
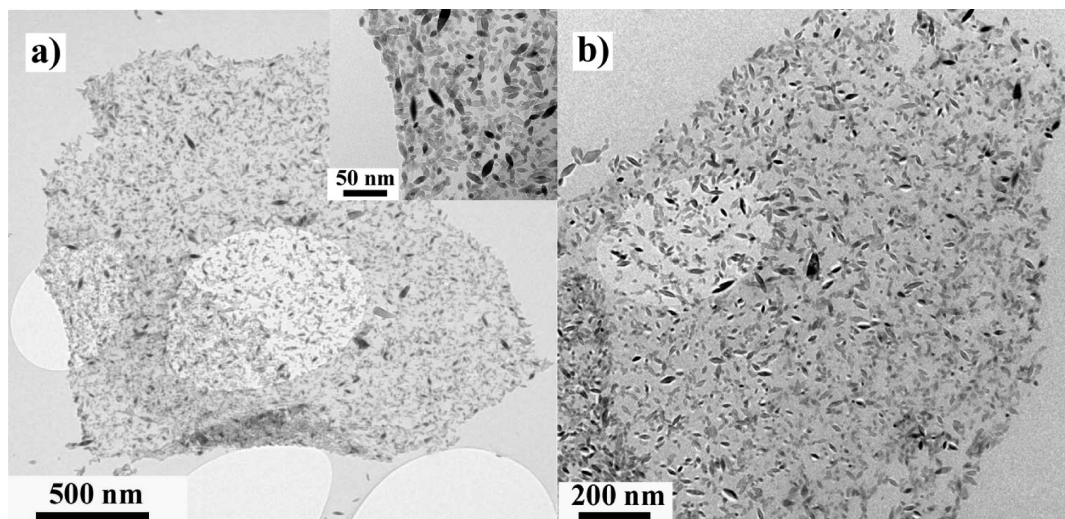
Figure 6. (a) A typical TEM image of a TiO_2 nanospindles/graphene oxide nanocomposite. (b) A TEM image of a $TiO_2@TiO_xN_y/TiN-GS$ nanocomposite after annealing in NH_3. Inset: A close-up view of the TEM image in panel A.

graphene is maintained after the thermal treatment in NH_3. In addition, comparison of the FT-IR bands of the as-prepared three samples (see Supporting Information, Figure S4) showed the absence of some characteristic functional groups of graphene oxide after forming the TiO_2/graphene nanocompsoite, but accompanied by a new peak at around 750 cm^{-1}, ascribable to the vibration of Ti–O groups.

To estimate the surface composition of the TiO_2 nanospindles, we refer to the XPS spectra in the core

level regions of Ti 2p and N 1s (Figure 7). The Ti 2p peak exhibits a unique doublet at around 458.5–464.5 eV, which is typical of Ti^{4+} in an octahedral environment. After the thermal nitridation, however, a new Ti 2p doublet at lower binding energies (454.5–459.5 eV) appears, which can be attributed to the formation of titanium nitride (TiN) (454.5–455.5 eV) and titanium oxynitride (TiO_xN_y) (456.0–456.7 eV) (Figure 7a).[50,51] Similarly, the N 1s peak also presents a doublet at around 395.1–402.3 eV, which is almost absent before the ni-
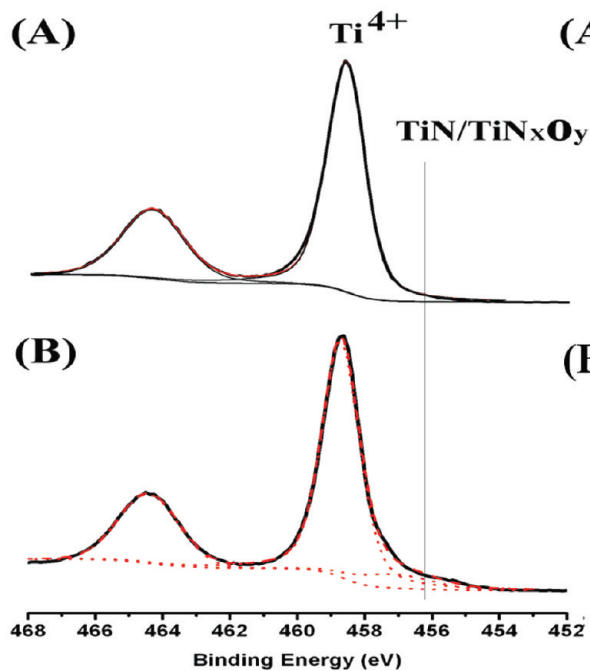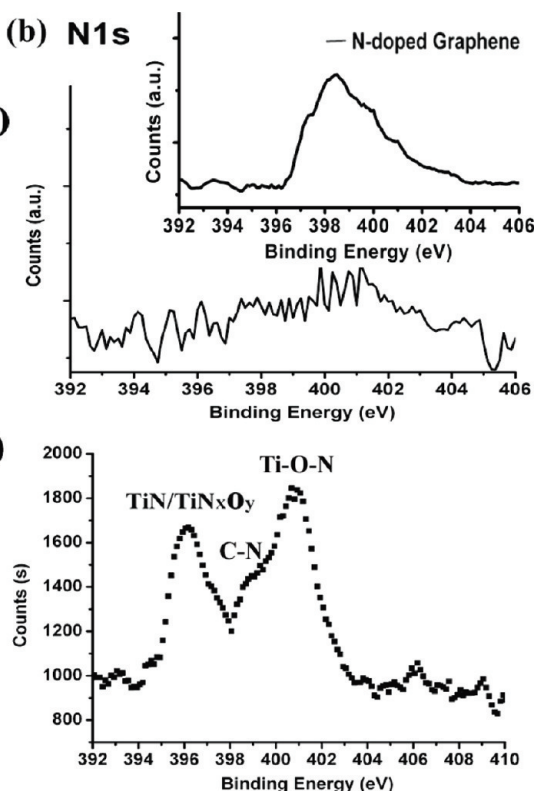

Figure 7. Ti $2p_{3/2,1/2}$ (a) and N 1s (b) XPS spectra of the TiO_2 nanospindle/graphene nanocomposite before (A) and after (B) nitridation at 650 °C. The fitted results are shown as red dashed curves. Top-right inset: N 1s XPS spectrum of the GO after annealing in NH_3 (N-doped graphene).

tridation (Figure 7b). Plausibly, the lower energy feature at around 395.1−399.7 eV is ascribed to the nitride and oxynitride species on the surface of the TiO_2 nanospindles, while the higher energy feature at around 400.9−402.3 eV is assigned to the characteristic energy losses or chemisorbed NH_x on the formed Ti−O−N species; the small shoulder in the middle energy range of 399.7−400.9 eV is mainly due to the C−N species of the N-doped graphene (see the inset of Figure 7b).[50,51]

Thermogravimetric analysis (TGA) was also conducted to investigate the content of graphene sheets in the as-prepared $TiO_2@TiO_xN_y/TiN−GS$ nanocomposite in air (Figure S6, Supporting Information). The first weight loss of ∼0.8% from 25 to 100 °C can be attributed to the loss of water adsorbed on the surface of the hybrid nanocomposite. The subsequent weight loss of ∼3% may be ascribed to the evaporation or/and oxidation of very small sized or defected graphene/carbon species. Starting from 300 up to 440 °C, the gradual weight increase of ∼1.6% corresponds to the oxidation of TiO_xN_y and TiN into TiO_2. Finally, a sharp weight loss of ∼7.0% from 440 to 530 °C can then be attributed to the complete combustion of the graphene sheets. Therefore the TGA data show that the graphene carbon content is ∼10% in the nanocomposite and they also confirm the formation of a thin layer of TiO_xN_y and/or TiN on the TiO_2 nanospindle surfaces.

Li Insertion/Extraction in the Nanocomposites. To demonstrate the effects of titania nanospindle size, surface nitridation, and hybridization with graphene sheets on the Li insertion/extraction properties, we fabricated electrodes consisting of TiO_2 nanospindles with different sizes and after different treatments. The electrodes were then used to make coin cells together with a Super P carbon additive and a PVDF binder, which are components of conventional Li-ion batteries. Shown in Figure 8a are the electrochemical behaviors of TiO_2 nanospindles of different sizes. One witnesses a distinct difference in Li-insertion behavior among the different-sized nanospindles. For example, at a rate of C/5, about 0.37 and 0.43 Li per TiO_2 (one Li insertion into TiO_2 ($LiTiO_2$) corresponds to a capacity of 336 mA h g^{-1}) are inserted into the samples of SP-200 and SP-100, respectively, which are apparently lower amounts than what is inserted into SP-20 (∼0.49 Li per TiO_2). Here the 1C-rate is defined as the current density necessary to fully charge/discharge the battery in 1 h. The nanospindle size-dependent Li insertion characteristics are corroborated by the subsequent discharge−charge curves. Obviously, the electrochemical behavior depends to a large extent on the particle size. This is understandable because in nanostructured systems, the Li surface storage may play a crucial role in the overall capacity, and such a Li insertion mechanism can be energetically more favorable for smaller nanoparticles than for large nanoparticles.[7,52]
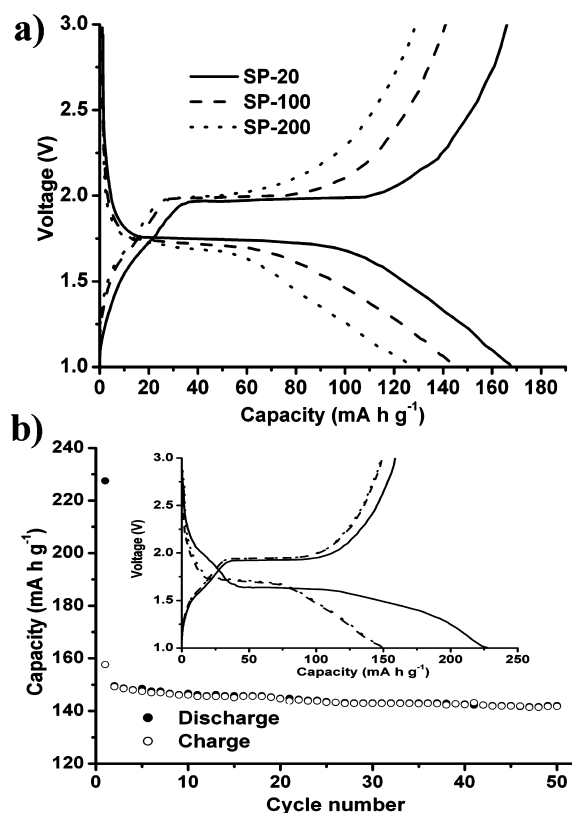

Figure 8. (a) Voltage profiles of the electrodes made of nanospindles with different sizes and shapes cycled at a rate of C/5 between 1.0 and 3.0 V. (b) Cycling performance of the electrode made of SP-20 at a rate of 1C. The inset shows the voltage profiles of the electrode made of SP-20 for the first three cycles in the range of 1−3 V.

Figure 8b displays room temperature cycling performance of SP-20 at a rate of 1C and in a potential range of 1.0−3.0 V. In the corresponding capacity−voltage curves for the first three cycles (inset of Figure 8b), the discharging plateaus at around 1.75 V and the charging plateau at around 1.9 V can be distinguished and ascribed, respectively, to Li-ion insertion and extraction, similar to those observed previously with nanoparticulate anatase.[53,54] The plateaus are associated with the phase transition between the tetragonal (anatase TiO_2) and orthorhombic (Li_xTiO_2) phases. From Figure 8b, one can also see a large irreversible capacity loss from the first to the second cycle, which is also observed in other anatase TiO_2.[53−55] Afterward, however, the capacity−voltage profiles show a steady voltage evolution with a constant potential region probably because a special structure may have been formed. Such a structure would be electrochemically reversible during Li insertion/extraction cycles, leading to a good capacity retention. As it happens, the average capacity loss per cycle is less than 0.18 mA h g^{-1} from the second to the 50th cycles at a rate of 1C.

To examine the effectiveness of the $TiO_2@TiO_xN_y/$ TiN and $TiO_2@TiO_xN_y/TiN−GS$ nanocomposite electrodes for LIBs, we also investigated their electrochemical properties with respect to Li-ion insertion/
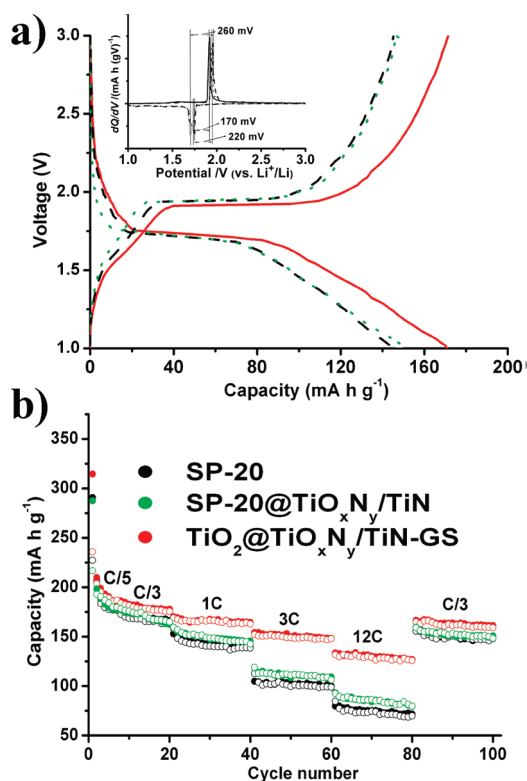
Figure 9. a) Voltage profiles of the electrodes made of SP-20 (black lines), and SP-20@TiO$_x$N$_y$/TiN (green lines), and TiO$_2$@TiO$_x$N$_y$/TiN−GS nanocomposite (red lines) cycled at a rate of 1C between 1.0 and 3.0 V. The inset in panel a shows the corresponding capacity derivatives with respect to voltage (dQ/dV). (b) Cycling specific capacity profiles of SP-20, SP-20@TiO$_x$N$_y$/TiN, and TiO$_2$@TiO$_x$N$_y$/TiN−GS nanocomposite at different charge/discharge rates.

extraction. For this purpose, we used the nanocomposite with the attached TiO$_2$ nanospindles having a diameter of ∼10 nm and a length of ∼20 nm because the size is comparable to those of SP-20 and SP-20@TiO$_x$N$_y$/TiN and thus allows a meaningful comparison. The Li insertion/extraction properties of the hybrid nanocomposite were investigated in the potential range of 1.0−3.0 V (*vs* Li$^+$/Li) for the Li storage in TiO$_2$,[12,13] which is above the reversible Li storage potential in graphene sheets (<1 V). Figure 9a displays the comparison discharge/charge profiles of the three materials cycled at a rate of 1C. The Li storage capacity in the TiO$_2$@TiO$_x$N$_y$/TiN−GS hybrid nanocomposite electrode is up to 166 mA h g^{-1}. This value is much larger than those of SP-20 (145 mA h g^{-1}) and SP-20@TiO$_x$N$_y$/TiN (150 mA h g^{-1}) due to the added conductive TiN/TiO$_x$N$_y$ thin layer and the underlying anchoring graphene sheets. In support of the beneficial role of the conductive graphene sheets, a much lower polarization has been achieved with the TiO$_2$@TiO$_x$N$_y$/TiN−GS nanocomposite (*ca.* 170 mV) than those of the pure TiO$_2$ nanospindles of SP-20 (*ca.* 260 mV) and SP-20@TiO$_x$N$_y$/TiN (*ca.* 220 mV), as can be seen from Figure 9a and the inset in Figure 9a. By the same token, the lower polarization for SP-20@TiO$_x$N$_y$/TiN (pure SP-20 after nitridation) than that of the

pure TiO$_2$ nanospindles of SP-20 speaks for the positive effect of the conductive TiO$_x$N$_y$/TiN sheath on the lithium insertion/extraction kinetics.

Figure 9b compares the rate performance of the three nanomaterials. All of the three electrodes were first cycled at a rate of C/5. Irreversible capacity losses in going from the first to the second cycle were observed for the three nanomaterials presumably due to decomposition of the electrolyte and/or solvent. Nevertheless, the initial discharge capacity of ∼314 mA h g^{-1} for the TiO$_2$@TiO$_x$N$_y$/TiN−GS is higher than those for the SP-20 (∼287 mA h g^{-1}) and for the SP-20@TiO$_x$N$_y$/TiN (∼290 mA h g^{-1}), which should be mainly credited to the improved lithium insertion/extraction kinetics in the TiO$_2$ nanospindles due to the added conductive TiN/TiO$_x$N$_y$ thin layer and the underlying anchoring graphene sheets. Especially notable is the excellent rate performance of the TiO$_2$@TiO$_x$N$_y$/TiN−GS hybrid nanocomposite compared with SP-20 and SP-20@TiO$_x$N$_y$/TiN. At a rate of C/3, the specific capacity of the TiO$_2$@TiO$_x$N$_y$/TiN−GS nanocomposite electrode was 175 mAh g^{-1}, which was slowly reduced to 166 mAh g^{-1} at 1C, 150 mAh g^{-1} at 3C, 130 mAh g^{-1} at 12C and finally resumed ∼165 mAh g^{-1} when the rate was reduced back to C/3. These capacities are to be compared to those of the electrode made of SP-20@TiO$_x$N$_y$/TiN under the same conditions, namely, only ∼149 mAh g^{-1} at 1C, ∼110 mAh g^{-1} at 3C, and ∼86 mA g^{-1} at 12C. This clearly is a positive effect of the graphene sheets on the rate performance. Actually, even lower specific capacities have been revealed for the electrode derived from SP-20. Those values were only ∼145 mAh g^{-1} at 1C, ∼105 mAh g^{-1} at 3C, and ∼75 mA g^{-1} at 12C. This highlights the benefit of the conductive layer of TiO$_x$N$_y$/TiN from the thermal nitridation process. Moreover, the good cycling performance of our TiO$_2$@TiO$_x$N$_y$/TiN−GS hybrid nanocomposite electrode also stands out when compared to the recent report by Wang *et al*. for a TiO$_2$/graphene hybrid composite with a capacity of ∼160 mA h g^{-1} at 1C, ∼135 mA h g^{-1} at 3C, and ∼120 mA h g^{-1} at 10C (1C = 168 mA h g^{-1}).[37] Although many factors, for example, the thickness of the electrode, the impedance of the electrode, *etc*., may contribute to the superior performance of our hybrid nanocomposite, the ordered dispersion of dense ultrafine TiO$_2$ nanospindles onto conductive graphene nanosheets in tandem with the thin TiN/TiO$_x$N$_y$ layer on the nanospindles are undoubtedly key to the capacity retention on cycling, especially at high discharge/charge rates.

CONCLUSIONS

We have combined synthesis, assembly, and device function to realize a high cycling performance LIB electrode by taking advantages of nanostructuring design and tailoring material hybridization. At the first level is the synthesis of size-tunable anatase TiO$_2$ nanospindles

via a hydrothermal dissolution/recrystallization process by using the tubular titanates as the source precursors. The size-tunability was achieved by the judicious choice of reaction solvents. The second level is characterized by the successful anchorage of the ultrafine anatase TiO_2 nanospindles onto graphene oxides in a uniform fashion to form TiO_2 nanospindles/graphene oxides hybrid nanostructures. Finally on the top, we have achieved significantly enhanced Li-ion insertion/

extraction performance with the hybrid nanocomposite after nitridation, especially at high charge/discharge rates. We anticipate that the size tunable TiO_2 nanospindles shall find applications in other areas such as sensors and solar cells. From the general perspective of methodology, the approach adopted in this work, which integrates synthesis, assembly, and functionalization, is going to prevail in the future bottom-up nanotechnology.

EXPERIMENTAL DETAILS

Synthesis of the Titanate Nanotube Precursor. In a typical synthesis, 0.4 g of TiO_2 (Degussa P25, about 20% rutile and 80% anatase with a particle size of about 20−30 nm) was dispersed in 20 mL of 10 M NaOH aqueous solution. After stirring for 30 min, the resulting suspension was transferred into a Teflon-lined stainless steel autoclave with a capacity of 100 mL. The autoclave was maintained at 150 °C for 20 h and then cooled to room temperature naturally. The resulting titanate nanotube precipitate was acid washed by adding a 0.1 M HCl solution under stirring until pH = 1−2, then filtered and washed again with distilled water several times.

Synthesis of TiO_2 Nanospindles with Different Sizes. To prepare TiO_2 nanospindles with different sizes (see Table 1), the titanate nanotube precursor was redispersed in 60 mL of different water and ethanol or ethylene glycol mixtures by stirring vigorously for 30 min. After adding 2 mL of dimethylamine, the stirring was continued for 30 min. The resulting mixture was sealed in a Teflon-lined stainless steel autoclave with a capacity of 100 mL and maintained at 180 °C for 12 h. After the autoclave was cooled to room temperature naturally, the turbid suspension inside the autoclave was centrifugally separated and the precipitate was collected.

Synthesis of TiO_2 Nanospindles/Graphene Oxides Nanocomposites. Graphene oxide (GO) sheets were prepared from natural graphite powder by oxidation with potassium permanganate according to the procedure reported by Hummers.[32] To disperse TiO_2 nanospindles onto graphene oxides, a procedure similar to that in the synthesis of the nanospindles described above was used, except that an appropriate amount of GO was added in the initial reaction mixture.

Synthesis of $TiO_2@TiO_xN_y/TiN$ Nanospindles and $TiO_2@TiO_xN_y/TiN−GS$ Nanocomposites by Thermal Nitridation. The TiO_2 nanospindles-graphene oxide nanocomposites prepared above (or using SP-20 TiO_2 to finally obtain $TiO_2@TiO_xN_y/TiN$ nanospindles) were loaded into a silica tube reactor placed in a horizontal tube furnace and connected to a gas feed system. Initially, a flow of Ar gas (99.99%) was maintained over the bed to get rid of air and H_2O. After a brief period (30 min) for stabilization of the gas flow, the furnace was heated from room temperature to 400 °C at a rate of 30 °C min^{-1}, held at this temperature for 30 min and then raised to 650 °C at a rate of 5 °C min^{-1}. Then, the flowing gas was switched to NH_3 with a flow rate of 30 cm^3 min^{-1}, and the reaction system was maintained at 650 °C for 15 min. Finally, the furnace was allowed to cool down under a flowing Ar gas.

Characterization. The as-prepared products were characterized by scanning electron microscopy (SEM), transmission electron microscopy (TEM), and powder X-ray diffraction (XRD) measurements. The morphologies were directly examined by SEM using a JEOL 6700F at an accelerating voltage of 5 kV. For TEM observations, the as-synthesized nanostructures were ultrasonically dispersed in ethanol and then dropped onto carbon-coated copper grids. TEM observations were carried out on JEOL 2010F and JEOL 2010 microscopes both operating at 200 kV. An energy-dispersive X-ray spectrometer (EDS) was attached to the JEOL 2010F. The XRD analyses were performed on a Philips PW-1830 X-ray diffractometer with Cu Kα radiation (λ = 1.5406 Å) at a scanning speed of 0.025°/sec over the 2θ range of 10−70°. The samples were in powder form dispersed on a carbon tape that

was attached to a sample holder. XPS spectra were measured on a Perkin-Elmer model PHI 5600 XPS system with a resolution of 0.3−0.5 eV from a monochromated aluminum anode X-ray source.

LIB Electrode Fabrication and Performance Measurements. The electrodes were fabricated by using the TiO_2 nanospindles and their nanocomposites as the active materials, conductive carbon blacks (Super-P) and polyvinylidene fluoride (PVDF) binder in a weight ratio of 75:15:10 and 85:5:10, respectively. The slurry was coated on a copper foil and dried overnight in a vacuum at 100 °C. For the square cell test, the electrode was cut into a square shape with an area of 1 cm^2. The electrochemical performances of these electrodes were evaluated in a 2016 coin-type TiO_2/Li cell, in which the lithium electrode was used as the counter electrode as well as the reference electrode. The electrolyte was 1 M $LiPF_6$ in ethylene carbonate (EC) and diethyl carbonate (DEC) (1:1 by volume). The charge/discharge tests were performed using an Arbin battery testing system at different current rates (1C = 168 mA g^{-1}) with a voltage window of 1−3 V.

Supporting Information Available: Additional SEM and TEM images showing the TiO_2 nanospindle formation process; FTIR and Raman spectra of the TiO_2/graphene nanocomposites. This material is available free of charge *via* the Internet at http://pubs.acs.org.

REFERENCES AND NOTES

1. Tollefson, J. Car Industry: Charging up the Future. *Nature* **2008**, *456*, 436–440.
2. Tarascon, J. M.; Armand, M. Issues and Challenges Facing Rechargeable Lithium Batteries. *Nature* **2001**, *414*, 359–367.
3. Arico, A. S.; Bruce, P.; Scrosati, B.; Tarascon, J.-M.; Schalkwijk, W. V. Nanostructured Materials for Advanced Energy Conversion and Storage Devices. *Nat. Mater.* **2005**, *4*, 366–377.
4. Idota, Y.; Kubota, T.; Matsufuji, A.; Maekawa, Y.; Miyasaka, T. Tin-Based Amorphous Oxide: A High-Capacity Lithium-Ion-Storage Material. *Science* **1997**, *276*, 1395–1397.
5. Armstrong, A. R.; Armstrong, G.; Canales, J.; Garcia, R.; Bruce, P. G. Lithium-Ion Intercalation into TiO_2-B Nanowires. *Adv. Mater.* **2005**, *17*, 862–865.
6. Armstrong, A. R.; Armstrong, G.; Canales, J.; Bruce, P. G. TiO_2-B Nanowires. *Angew. Chem., Int. Ed.* **2004**, *43*, 2286–2288.
7. Hu, Y.-S.; Kienle, L.; Guo, Y.-G.; Maier, J. High Lithium Electroactivity of Nanometer-Sized Rutile TiO_2. *Adv. Mater.* **2006**, *18*, 1421–1426.
8. Boschloo, G. K.; Goossens, A.; Schoonman, J. Photoelectrochemical Study of Thin Anatase TiO_2 Films Prepared by Metalorganic Chemical Vapor Deposition. *J. Electrochem. Soc.* **1997**, *144*, 1311–1317.
9. Wagemaker, M.; Kentgens, A. P. M.; Mulder, F. M.

Equilibrium Lithium Transport between Nanocrystalline Phases in Intercalated TiO_2 Anatase. *Nature* **2002**, *418*, 397–399.

10. Kavan, L.; Grätzel, M.; Gilbert, S. E.; Klemenz, C.; Scheel, H. J. Electrochemical and Photoelectrochemical Investigation of Single-Crystal Anatase. *J. Am. Chem. Soc.* **1996**, *118*, 6716–6723.

11. Liu, H.; Fu, L. J.; Zhang, H. P.; Gao, J.; Li, C.; Wu, Y. P.; Wu, H. Q. Effects of Carbon Coatings on Nanocomposite Electrodes for Lithium-Ion Batteries. *Electrochem. Solid-State Lett.* **2006**, *9*, A529–A533.

12. Guo, Y. G.; Hu, Y. S.; Sigle, W.; Maier, J. Superior Electrode Performance of Nanostructured Mesoporous TiO_2 (Anatase) through Efficient Hierarchical Mixed Conducting Networks. *Adv. Mater.* **2007**, *19*, 2087–2091.

13. Kavan, L.; Bacsa, R.; Tunckol, M.; Serp, P.; Zakeeruddin, S. M.; Le Formal, F.; Zukalova, M.; Graetzel, M. Multiwalled Carbon Nanotubes Functionalized by Carboxylic Groups: Activation of TiO_2 (Anatase) and Phosphate Olivines ($LiMnPO_4$; $LiFePO_4$) for Electrochemical Li-Storage. *J. Power Sources* **2010**, *195*, 5360–5369.

14. Adachi, M.; Murata, Y.; Takao, J.; Jiu, J.; Sakamoto, M.; Wang, F. Highly Efficient Dye-Sensitized Solar Cells with a Titania Thin-Film Electrode Composed of a Network Structure of Single-Crystal-like TiO_2 Nanowires Made by the "Oriented Attachment" Mechanism. *J. Am. Chem. Soc.* **2004**, *126*, 14943–14949.

15. Joo, J.; Kwon, S. G.; Yu, T.; Cho, M.; Lee, J.; Yoon, J.; Hyeon, T. Large-Scale Synthesis of TiO_2 Nanorods *via* Nonhydrolytic Sol−Gel Ester Elimination Reaction and Their Application to Photocatalytic Inactivation of *E. coli. J. Phys. Chem. B* **2005**, *109*, 15297–15302.

16. Kavan, L.; Kalbac, M.; Zukalova, M.; Exnar, I.; Lorenzen, V.; Nesper, R.; Graetzel, M. Lithium Storage in Nanostructured TiO_2 Made by Hydrothermal Growth. *Chem. Mater.* **2004**, *16*, 477–485.

17. Zukalová, M.; Kalbác, M.; Kavan, L.; Exnar, I.; Graetzel, M. Pseudocapacitive Lithium Storage in $TiO_2(B)$. *Chem. Mater.* **2005**, *17*, 1248–1255.

18. Indris, S.; Amade, R.; Heitjans, P.; Finger, M.; Haeger, A.; Hesse, D.; Grunert, W.; Borger, A.; Becker, K. D. Preparation by High-Energy Milling, Characterization, and Catalytic Properties of Nanocrystalline TiO_2. *J. Phys. Chem. B* **2005**, *109*, 23274–23278.

19. Liu, S. Q.; Chen, A. C. Coadsorption of Horseradish Peroxidase with Thionine on TiO_2 Nanotubes for Biosensing. *Langmuir* **2005**, *21*, 8409–8413.

20. Oh, S. H.; Finones, R. R.; Daraio, C.; Chen, L. H.; Jin, S. H. Growth of Nano-scale Hydroxyapatite Using Chemically Treated Titanium Oxide Nanotubes. *Biomaterials* **2005**, *26*, 4938–4943.

21. Qiu, Y. C.; Chen, W.; Yang, S. H. Double-Layered Photoanodes from Variable-Size Anatase TiO_2 Nanospindles: A Candidate for High-Efficiency Dye-Sensitized Solar Cells. *Angew. Chem., Int. Ed.* **2010**, *49*, 3675–3679.

22. Zhang, W. X.; Yang, S. H. *In Situ* Fabrication of Inorganic Nanowire Arrays Grown from and Aligned on Metal Substrates. *Acc. Chem. Res.* **2010**, *42*, 1617–1627.

23. Rao, C. N. R.; Deepak, F. L.; Gundiah, G.; Govindaraj, A. Inorganic Nanowires. *Prog. Solid State Chem.* **2003**, *31*, 5–147.

24. Xia, Y. N.; Yang, P. D.; Sun, Y. G.; Wu, Y. Y.; Mayers, B.; Gates, B.; Yin, Y. D.; Kim, F.; Yan, H. Q. One-Dimensional Nanostructures: Synthesis, Characterization, Applications. *Adv. Mater.* **2003**, *15*, 353–389.

25. Satyanarayana Kuchibhatla, V. N. T.; Karakoti, A. S.; Debasis, Bera.; Seal, S. One Dimensional Nanostructured Materials. *Prog. Mater. Sci.* **2007**, *52*, 699–913.

26. Chen, X. B.; Mao, S. S. Titanium Dioxide Nanomaterials: Synthesis, Properties, Modifications, and Applications. *Chem. Rev.* **2007**, *107*, 2891–2959.

27. Chu, R. H.; Yan, J. C.; Lian, S. Y.; Wang, Y. H.; Yan, F. C.; Chen, D. W. Shape-Controlled Synthesis of Nanocrystalline Titania at Room Temperature. *Solid State Commun.* **2004**, *130*, 78–792.

28. Ambrus, Z.; Mogyorosi, K.; Szalai, A.; Alapi, T.; Demeter, K.; Dombi, A.; Sipos, P. Low Temperature Synthesis, Characterization and Substrate-Dependent Photocatalytic Activity of Nanocrystalline TiO_2 with Tailor-made Rutile to Anatase Ratio. *Appl. Catal., A* **2008**, *340*, 153–161.

29. Yang, C.; Yang, Z. M.; Gu, H. W.; Chang, C. K.; Gao, P.; Xu, B. Facet-Selective 2D Self-Assembly of TiO_2 Nanoleaves *via* Supramolecular Interactions. *Chem. Mater.* **2008**, *20*, 7514–7520.

30. Wang, H. K.; Shao, W.; Gu, F.; Zhang, L.; Lu, M. K.; Li, C. Z. Synthesis of Anatase TiO_2 Nanoshuttles by Self-Sacrificing of Titanate Nanowires. *Inorg. Chem.* **2009**, *48*, 9732–9736.

31. Geim, A. K.; Novoselov, K. S. The Rise of Graphene. *Nat. Mater.* **2007**, *6*, 183–191.

32. Li, X. L.; Wang, X. R.; Zhang, L.; Lee, S. W.; Dai, H. J. Chemically Derived, Ultrasmooth Graphene Nanoribbon Semiconductors. *Science* **2008**, *319*, 1229–1232.

33. Wang, X. R.; Ouyang, Y. J.; Li, X. L.; Wang, H. L.; Guo, J.; Dai, H. J. Room-Temperature All-Semiconducting sub-10-nm Graphene Nanoribbon Field-Effect Transistors. *Phys. Rev. Lett.* **2008**, *100*, 206803.

34. Stoller, M. D.; Park, S. J.; Zhu, Y. W.; An, J. H.; Ruoff, R. S. Graphene-Based Ultracapacitors. *Nano Lett.* **2008**, *8*, 3498–3502.

35. Yoo, E. J.; Kim, J.; Hosono, E.; Zhou, H. S.; Kudo, T.; Honma, I. Large Reversible Li Storage of Graphene Nanosheet Families for Use in Rechargeable Lithium Ion Batteries. *Nano Lett.* **2008**, *8*, 2277–2282.

36. Paek, S. M.; Yoo, E.; Honma, I. Enhanced Cyclic Performance and Lithium Storage Capacity of SnO_2/Graphene Nanoporous Electrodes with Three-Dimensionally Delaminated Flexible Structure. *Nano Lett.* **2009**, *9*, 72–75.

37. Wang, D. H.; Choi, D. W.; Li, J.; Yang, Z. G.; Nie, Z. M.; Kou, R.; Hu, D. H.; Wang, C. M.; Saraf, L. V.; Zhang, J. G.; *et al.* Self-Assembled TiO_2-Graphene Hybrid Nanostructures for Enhanced Li-Ion Insertion. *ACS Nano* **2009**, *3*, 907–914.

38. Hummers, W. S.; Offeman, R. E. Preparation of Graphitic Oxide. *J. Am. Chem. Soc.* **1958**, *80*, 1339.

39. Liu, C. M.; Yang, S. H. Synthesis of Angstrom-Scale Anatase Titania Atomic Wires. *ACS Nano* **2009**, *3*, 1025–1031.

40. Liu, C. M.; Sun, H.; Yang, S. H. From Nanorods to Atomically Thin Wires of Anatase TiO_2: Nonhydrolytic Synthesis and Characterizations. *Chem.—Eur. J.* **2010**, *16*, 4381–4393.

41. Feng, Q.; Hirasawa, M.; Yanagisawa, K. Synthesis of Crystal-Axis-Oriented $BaTiO_3$ and Anatase Plate-like Particles by a Hydrothermal Soft Chemical Process. *Chem. Mater.* **2001**, *13*, 290–296.

42. Feist, T. P.; Davies, P. K. The Soft Chemical Synthesis of TiO_2 (B) from Layered Titanates. *J. Solid State Chem.* **1992**, *101*, 275–295.

43. Paek, M. J.; Ha, H. W.; Kim, T. W.; Moon, S. J.; Baeg, J. O.; Choy, J. H.; Hwang, S. J. Formation Efficiency of One-Dimensional Nanostructured Titanium Oxide Affected by the Structure and Composition of Titanate Precursor: A Mechanism Study. *J. Phys. Chem. C* **2008**, *112*, 15966–15972.

44. Xu, C. Y.; Zhang, Q.; Zhang, H.; Zhen, L.; Tang, J.; Qin, L. C. Synthesis and Characterization of Single-Crystalline Alkali Titanate Nanowires. *J. Am. Chem. Soc.* **2005**, *127*, 11584–11585.

45. Gao, W.; Alemany, L. B.; Ci, L. J.; Ajayan, P. M. New Insights into the Structure and Reduction of Graphite Oxide. *Nat. Chem.* **2009**, *1*, 403–408.

46. Hontoria-Lucas, C.; Lopez-Peinado, A. J.; Lopez-Gonzalez, J. deD.; Rojas-Cervantes, M. L.; Martin-Aranda, R. M. Study of Oxygen-Containing Groups in a Series of Graphite Oxides: Physical and Chemical Characterization. *Carbon* **1995**, *33*, 1585–1592.

47. Li, X.; Wang, H.; Robinson, J. T.; Sanchez, H.; Diankov, G.;

Dai, H. J. Simultaneous Nitrogen Doping and Reduction of Graphene Oxide. *J. Am. Chem. Soc.* **2009**, *131*, 15939–15944.

48. Park, K.-S.; Benayad, A.; Kang, D.-J.; Doo, S.-G. Nitridation-Driven Conductive $Li_4Ti_5O_{12}$ for Lithium Ion Batteries. *J. Am. Chem. Soc.* **2008**, *130*, 14930–14931.

49. Ohsaka, T.; Izumi, F.; Fujiki, Y. Raman Spectrum of Anatase TiO_2. *J. Raman Spectrosc.* **1978**, *7*, 321–324.

50. Livraghi, S.; Paganini, M. C.; Giamello, E.; Selloni, A.; Valentin, C. D.; Pacchioni, G. Origin of Photoactivity of Nitrogen-Doped Titanium Dioxide under Visible Light. *J. Am. Chem. Soc.* **2006**, *128*, 15666–15671.

51. Zukalova, M.; Prochazka, J.; Bastl, Z.; Duchoslav, J.; Rubacek, L.; Havlicek, D.; Kavan, L. Facile Conversion of Electrospun TiO_2 into Titanium Nitride/Oxynitride Fibers. *Chem. Mater.* **2010**, *22*, 4045–4055.

52. Wagemaker, M.; Borghols, W. J. H.; Mulder, F. M. Large Impact of Particle Size on Insertion Reactions. A Case for Anatase Li_xTiO_2. *J. Am. Chem. Soc.* **2007**, *129*, 4323–4327.

53. Sudant, G.; Baudrin, E.; Larcher, D.; Tarascon, J. M. Electrochemical Lithium Reactivity with Nanotextured Anatase-type TiO_2. *J. Mater. Chem.* **2005**, *15*, 1263–1269.

54. Jiang, C. H.; Wei, M. D.; Qi, Z. M.; Kudo, T.; Honma, I.; Zhou, H. S. Particle Size Dependence of the Lithium Storage Capability and High Rate Performance of Nanocrystalline Anatase TiO_2 Electrode. *J. Power Sources* **2007**, *166*, 239–243.

55. Yang, Z.; Choi, D.; Kerisita, S.; Rossoa, K. M.; Wang, D.; Zhang, J.; Graff, G.; Liu., J. Nanostructures and Lithium Electrochemical Reactivity of Lithium Titanites and Titanium Oxides: A Review. *J. Power Sources* **2009**, *192*, 588–598.